Spatial Electrochromism in Metallopolymeric Films of Ruthenium Polypyridyl Complexes

Robert M. Leasure, Wei Ou, John A. Moss, Richard W. Linton, and Thomas J. Meyer*

The University of North Carolina, Department of Chemistry, Venable Hall, CB#3290, Chapel Hill, North Carolina 27599-3290

Received August 8, 1995. Revised Manuscript Received September 27, 1995[⊗]

Thin films of poly$[Ru(vbpy)_2(py)_2]^{2+}$ (vbpy is 4-vinyl-4′-methyl-2,2′-bipyridine; py is pyridine) have been deposited on electrodes by reductive electropolymerization. Photolysis of the films in the presence of chloride ion leads to photochemical loss of the pyridine ligands and sequential formation of poly$[Ru(vbpy)_2(py)Cl]^{+}$ and poly$[Ru(vbpy)_2Cl_2]$, as determined by cyclic voltammetry and FTIR spectroscopy. Contact lithography was used to control the photosubstitution process spatially and form laterally resolved, bicomponent films with image resolution below 10 μm. Small spot X-ray photoelectron spectroscopy (XPS) was used to confirm that the photolyzed and nonphotolyzed regions of an imaged film were chemically distinct. Dramatic changes occur in the absorption spectra and redox potentials of the ruthenium complexes upon substitution of chloride for the pyridine ligands. This provides a basis for the fabrication of bicomponent, electrochromic film assemblies on optically transparent electrodes of tin doped indium oxide on glass. The spectroelectrochemical response of these films has been studied by slow scan cyclic voltammetry and potential step chronoamperometry.

Introduction

Techniques are well established for the preparation of submicron polymeric films containing polypyridyl complexes of Ru^{II}, Os^{II}, and Fe^{II}.[1−3] The metal complex units have characteristic redox and absorption properties which can be varied systematically by changing the surrounding ligands.[4−7] Potentials for $M^{III/II}$ couples can be varied over 1.0 V and absorptivity from the low energy visible to near UV.[4] Elliott and co-workers have demonstrated that cast films of poly[ruthenium (5,5′-bis[acryl-1-propoxy-carbonyl]-2,2′-bipyridine)$_3$]$^{2+}$ undergo up to seven reversible oxidation state changes, with corresponding color changes distinctly different at each stage.[8] Their work points to the use of these redox polymeric films as electrochromic displays.

Photochemical ligand substitution is well established for $[Ru^{II}(bpy)_2(py)_2]^{2+}$ (bpy is 2,2′-bipyridine, py is pyridine) in solution[9] and has been extended to redox polymeric films of poly(4-vinylpyridine) containing pendant Ru^{II} complexes.[10−12] We have combined electropolymerization and photosubstitution techniques to develop procedures for imaging and microstructure formation in films containing polypyridylmetal complexes.[13] The imaging is based on lithographic techniques and the photolability of the Ru−vpy bonds in films of poly$[Ru^{II}(tmb)_2(vpy)_2]^{2+}$ (where tmb is 4,4′,5,5′-tetramethyl-2,2′-bipyridine, vpy is 4-vinylpyridine; Scheme 1). By exploiting the substituent effects of the electron donating methyl groups in the tmb ligand, it was possible to deposit a second polymer by selective electropolymerization within the photolyzed regions of the inital film.[13−15]

We have also described a procedure for preparing spatially defined, bicomponent films based on masking techniques and ligand substitution in photochemically stable films.[16] Photosubstitution occurs in films of poly$[Ru^{II}(vbpy)_2(py)_2]^{2+}$ (vbpy is 4-methyl-4′-vinyl-2,2′-bipyridine; Scheme 2), but the cross-linking is not disrupted and the films remain intact. In this paper, we extend this work and apply lithographic techniques to prepare bicomponent film assemblies which display spatially controllable electrochromism.

Experimental Section

Materials. For electrochemical measurements, acetonitrile (Burdick & Jackson) was bubble degassed and

* To whom correspondence should be addressed.

[⊗] Abstract published in *Advance ACS Abstracts,* November 1, 1995.

(1) Abruña, H. D. *Coord. Chem. Rev.* **1988**, *86*, 135−189.
(2) Merz, A. In *Topics in Current Chemistry—Electrochemistry IV*; Steckhan, E., Ed.; Springer-Verlag: Berlin, 1990; Vol. 152; pp 49−90.
(3) *Molecular Design of Electrode Surfaces*; Murray, R. W., Ed.; John Wiley & Sons, Inc.: New York, 1992; Vol. XXII.
(4) Juris, A.; Balzani, V.; Barigelletti, F.; Campagna, S.; Belser, P.; Zelewsky, A. V. *Coord. Chem. Rev.* **1988**, *84*, 85−277.
(5) Meyer, T. J. *Acc. Chem. Res.* **1989**, *22*, 163−170.
(6) Balzani, V.; Scandola, F. *Supramolecular Photochemistry*; Ellis Harwood: Chister, 1990.
(7) Kalyansasundarum, K. *Photochemistry of Polypyridines and Porphyrins* Academic Press: London, 1992.
(8) Elliott, C. M.; Schmittle, S. J.; Redepenning, J. G.; Balk, E. M. *J. Macromol. Sci., Chem.* **1988**, *A25*, 1215−1225.
(9) Durham, B.; Walsh, J. L.; Carter, C. L.; Meyer, T. J. *Inorg. Chem.* **1980**, *19*, 860−865.
(10) Haas, O.; Kriens, M.; Vos, J. G. *J. Am. Chem. Soc.* **1981**, *103*, 1318−1319.
(11) Haas, O.; Zumbrunnen, H. R.; Vos, J. G. *Electrochimi. Acta* **1985**, *30*, 1551−1554.
(12) Calvert, J. M.; Meyer, T. J. *Inorg. Chem.* **1982**, *21*, 3978−3989.
(13) Gould, S.; O'Toole, T. R.; Meyer, T. J. *J. Am. Chem. Soc.* **1990**, *112*, 26.
(14) Gray, K. H.; Gould, S.; Leasure, R. M.; Musselman, I. H.; Lee, J. J.; Meyer, T. J.; Linton, R. W. *J. Vac. Sci. Technol. A* **1992**, *10(4)*, 2679−2684.
(15) Leasure, R. M.; Moss, J. A.; Meyer, T. J. *Inorg. Chem.* **1994**, *33*, 1247−1248.
(16) Leasure, R. M.; Ou, W.; Moss, J. A.; Linton, R. W.; Meyer, T. J. In *Proceedings of the Symposium on Electrochromic Materials II at The 184th Meeting of The Electrochemical Society*; The Electrochemical Society: New Orleans, 1994; pp 222−234.

0897-4756/96/2808-0264$12.00/0 © 1996 American Chemical Society

Scheme 1

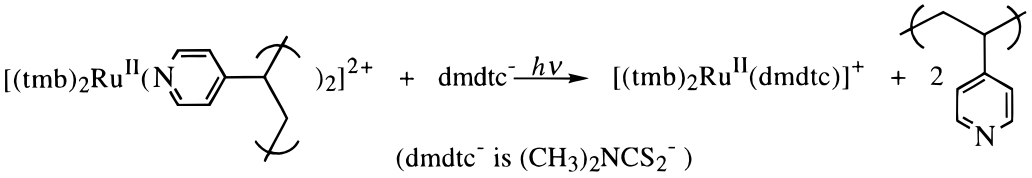

Scheme 2

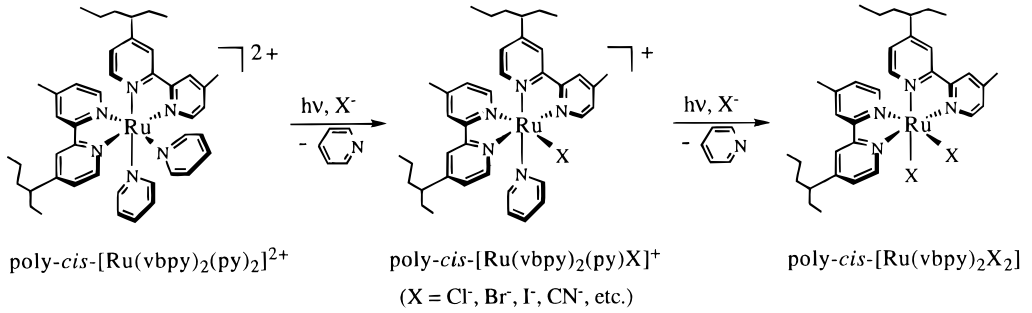

stored under nitrogen. Dichloromethane was dried over P_2O_5 and freshly distilled. For synthetic work, all chemicals and solvents were reagent grade or better. Tetra-*n*-butylammonium hexafluorophosphate (TBAH) was prepared by adding a stoichiometric amount of hexafluorophosphoric acid (Aldrich) to an aqueous solution of tetra-*n*-butylammonium bromide (Aldrich). The resulting precipitate was recrystallized twice from absolute ethanol and dried in vacuo at 60 °C for 2 days (mp 246−248 °C). Tetra-*n*-butylammonium chloride (Aldrich) was purified according to a literature method[17] and stored under nitrogen. The monomeric analogues, $[Ru^{II}(dmb)_2(py)_2](PF_6)_2$ and $Ru^{II}(dmb)_2Cl_2{\cdot}2H_2O$ (dmb is 4,4′-dimethyl-2,2′-bipyridine, Sigma) were prepared by using the synthetic procedures for the vbpy complexes described below. $[Ru^{II}(dmb)_2(py)Cl](PF_6){\cdot}H_2O$ was prepared by modification of a literature procedure,[18] with dmb instead of bpy. 4-Carboxyaldehyde-4′-methyl-2,2′-bipyridine (bpy−CHO) was prepared according to a literature procedure.[19]

Teflon shrouded platinum disk electrodes (0.12 cm^2) were constructed according to a previously described procedure.[20] They were polished prior to use with 1 μm diamond paste (Buehler) on a Gould 550/1140 rpm polishing wheel (Buehler). Spectroelectrochemical measurements were conducted on optically transparent electrodes of tin-doped indium oxide (ITO) coated on glass (Delta Technologies, Ltd.) and were sonicated for 20 min in dichloromethane prior to use. FTIR spectra of polymeric films were obtained by using polished flags of platinum as the conducting substrate.

Syntheses. *4-Vinyl-4′-methyl-2,2′-bipyridine (vbpy).* A modified procedure for the preparation of vbpy to those reported in the literature was used.[21,22] To a suspension of 2.72 g (7.6 mmol) of methyltriphenylphosphonium bromide in 100 mL of freshly distilled tetrahydrofuran at 0 °C was added 3.5 mL of a 2.5 M solution of *n*-butyllithium in hexanes (Aldrich). The resulting yellow solution was stirred for 30 min then cooled to −78 °C in a dry ice/acetone bath. To it was added 1.5 g (7.6 mmol) of 4-carboxaldehyde-4′-methyl-2,2′-bipyridine dissolved in 100 mL of THF via canula. After warming to room temperature, 100 mL of distilled H_2O was added, and the THF was removed by rotary evaporation. The colorless aqueous solution was extracted three times with 100 mL aliquots of dichloromethane. The nonaqueous layers were combined and back extracted with 1 M NaCl. The dichloromethane layer was dried over $NaSO_4$, filtered, and evaporated to dryness. The resuting colorless solid was purified on a column of neutral aluminum (Fisher) with 1:4 ethylacetate/hexane as the eluent. The overall yield was 33%.

^{1}H NMR (δ(ppm), CD_3Cl) 8.54 (d, J_{56} = 5.11 Hz, 1H, H_6); 8.18 (d, $J_{5'6'}$ = 3.40 Hz, 1H, $H_{6'}$); 8.32 (s, 1H, H_3); 8.17 (s, 1H, $H_{3'}$); 7.24 (d, J_{65} = 3.59 Hz, 1H, H_5); 7.08 (d, $J_{6'5'}$ = 4.80 Hz, 1H, $H_{5'}$); 6.69 (dd, J_{AX} = 17.6 Hz and J_{BX} = 10.6, 1H, H_x); 6.02 (d, J_{XA} = 19.6 Hz, 1H, H_A); 5.45 (d, J_{XB} = 10.8 Hz, 1H, H_B); 2.37 (s, 3H, H_{methyl}).

$Ru^{II}(vbpy)_2Cl_2{\cdot}2H_2O$. A nitrogen-deaerated solution of 2:1 dimethoxyethane/methanol containing 200 mg (0.964 mmol) of $RuCl_3{\cdot}3H_2O$ (Aldrich), 378 mg (1.93 mmol) of vbpy, 265 mg (2.41 mmol) hydroquinone, and 1.23 g (29 mmol) of LiCl was heated at reflux for 5 h under N_2. After cooling, the solution was reduced in volume under vacuum, dissolved in 500 mL of CH_2Cl_2, and washed with five 100 mL aliquots of distilled water. The dichloromethane layer was dried over $NaSO_4$, filtered, and rotary evaporated to dryness. The product was reprecipitated from a minimum volume of dichloromethane by dropping into stirring diethyl ether. The product was collected as a purple powder; yield 75%.

Anal. Calcd for $Ru(vbpy)_2Cl_2{\cdot}2H_2O$: C, 52.00; H, 9.33; N, 4.70. Found: C, 50.99; H, 9.04; N, 4.26.

$[Ru^{II}(vbpy)_2(py)_2](PF_6)_2$. To a nitrogen degassed solution of 200 mg (0.333 mmol) of $Ru^{II}(vbpy)_2Cl_2{\cdot}2H_2O$ in 50 mL of 1:1 methanol/water was added 2 mL of pyridine. The solution was heated at reflux for 3 h in the dark under an atmosphere of N_2. The solution was cooled to room temperature, and to it was added 50 mL of distilled water and a few milliliters of a saturated

(17) Perin, D. D.; Armarego, W. L. F. *Purification of Laboratory Chemicals*, 3rd ed.; Pergamon Press: Oxford, 1992.
(18) Moyer, B. A.; Meyer, T. J. *Inorg. Chem.* **1981**, *20*, 436−444.
(19) Peek, B. M.; Ross, G. T.; Edwards, S., W.; Meyer, G., J.; Meyer, T. J.; Erickson, B. W. *Int. J. Peptide Protein Res.* **1991**, *38*, 194.
(20) Brandt, E. S. Ph.D. Thesis, University of North Carolina at Chapel Hill, 1978.
(21) Abruña, H. D.; Breikss, A. I.; Collum, D. B. *Inorg. Chem.* **1985**, *24*, 987−989.
(22) Guarr, T. F.; Anson, F. C. *J. Phys. Chem.* **1987**, *91*, 4037−4043.

Scheme 3

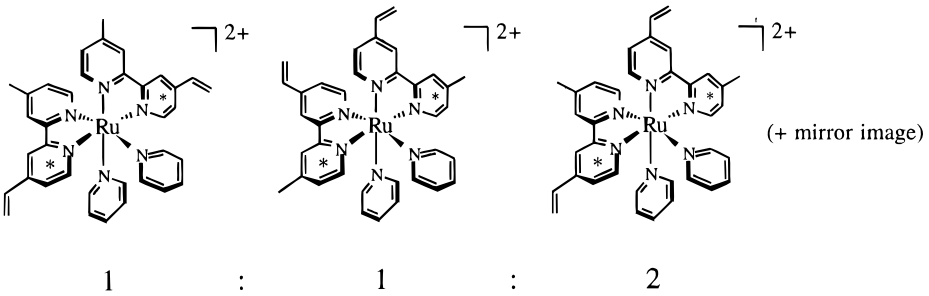

1 : 1 : 2

aqueous solution of NH_4PF_6. An orange precipitate formed and was collected on a medium glass frit. The product was purified on alumina eluting with 1:1 toluene/acetonitrile, collecting the second, trailing band. The solvent was evaporated under vacuum, and the product was reprecipitated from a minimum volume of acetonitrile by dropping into stirring diethyl ether. The product was collected as an orange powder, yield 38%.

Anal. Calcd for $[Ru(vbpy)_2(py)_2](PF_6)_2$: C, 45.92; H, 8.98; N, 3.64. Found: C, 45.27; H, 8.65; N, 3.59.

^{1}H NMR (δ(ppm), CD_3CN) 8.78 (d, $J_{5*6*} = 5.9$ Hz, 1H, H_{6}^{*}); 8.69 (d, $J_{5'*6'*} = 5.2$ Hz, 1H, $H_{6'}^{*}$); 8.42−8.18 (m, 8H, 4H$_\alpha$, H_3, H_3^*, $H_{3'}$, $H_{3'}^*$); 7.87−7.58 (m, 6H, 2H$_\gamma$, H_5^*, H_6, $H_{5'}^*$, $H_{6'}$); 7.38−7.18 (m, 6H, 4H$_\beta$, H_5, $H_{5'}$); 6.92 (dd, $J_{X*A*} = 17.6$ Hz, $J_{X*B*} = 11.6$, 1H, H_x^*); 6.77 (dd, $J_{AX} = 17.8$ Hz, $J_{BX} = 10.6$, 1H, H_x); 6.36 (d, $J_{X*A*} = 17.8$ Hz, 1H, H_A^*); 6.22 (d, $J_{XA} = 17.5$ Hz, 1H, H_A); 5.75 (d, $J_{X*B*} = 11.2$ Hz, 1H, H_B^*); 5.65 (d, $J_{XB} = 10.7$ Hz, 1H, H_B); 2.59 (s, 3H, CH_3^*); 2.44 (s, 3H, CH_3). Note: The asteriks indicate protons on the bipyridyl rings that are adjacent to both pyridine ligands, as shown in Scheme 3.

Instrumentation and Equipment. ^{1}H NMR spectra were acquired with a Varian XL400 spectrometer in CD_3Cl or CD_3CN (Cambridge Isotopes). Cyclic voltammetric and chronoamperometric experiments were carried out by using Princeton Applied Research Model 273 or Model 263 potentiostat/galvanostats interfaced to an IBM compatible personal computers. Electrochemical experiments were carried out in acetonitrile or dichloromethane solutions containing either 0.1 or 0.2 M TBAH as the supporting electrolyte with a nonaqueous $Ag/AgNO_3$ reference electrode, which was 0.01 M $AgNO_3$/Ag in 0.1 M TBAH/CH_3CN. Its potential vs the saturated sodium chloride calomel electrode (SSCE) was +0.30 ± 0.03 V. Potentials are reported relative to the SSCE and were converted by comparing the open-circuit potential between the two references or by monitoring the half-wave potential of $[Ru(bpy)_2Cl_2]^{+/0}$ couple (+0.34 V vs SSCE in CH_3CN). Electropolymerizations were carried out in a Vacuum Atmospheres glovebox modified to operate under a constant N_2 purge. Two compartment electrochemical cells were designed such that a platinum mesh counter electrode was reproducibly positioned parallel to and opposite the working electrode. This arrangement provided a uniform current density over the entire surface of the working electrode allowing for more homogeneous film growth.

Broad-band photolyses were carried out with a Bausch & Lomb SP200 high-pressure 200 W mercury lamp. The output of the lamp was passed through a Pyrex UV cutoff filter and collimated through a 14 cm path length water filter for reduction of IR heating. The light beam was focused onto one end of a 5 mm core liquid light guide (Oriel Corp.) to homogenize the output light beam and simplify manipulations required for positioning of the optical masks and electrodes.

Optical masks for photolithography were prepared from high contrast 35 mm slide film (Kodak LPD-4) which allowed the imaging pattern to be easily controlled. Higher resolution images were obtained by using a commercially available resolution test target of chrome plated onto optical grade crown glass (USAF 1951, Oriel Corp.).

Specular reflectance infrared spectra[23] were aquired with a Mattson Galaxy Series Model 5000 Fourier transform infrared (FTIR) spectrometer equipped with a liquid N_2 cooled mercury cadmium telluride (MCT) detector. The angle of incidence of the specular reflectance attachment (Harrick Scientific Corp.) was fixed at 75°.

X-ray photoelectron spectra (XPS) were acquired on a Perkin-Elmer Physical Electronics Model 5400 spectrometer. The operating conditions were as follows: Mg Kα anode (15 kV, 400 W); hemispherical analyzer (pass energy 35 eV); angle of collection 45°; analysis area 0.95 mm^2; base pressure 3×10^{-8} Torr. Binding energies were charge referenced to the C 1s peak at 285 eV. Photoelectron spectra were interpreted by using a standard curve-fit routine (80% Gaussian and 20% Lorenztian) with a Shirley background subtraction.[24] Quantitative atomic percentages were calculated by using instrumental relative sensitivity factors (RSF) and integrated photoelectron peak areas. RSF values were obtained from spectra of purified samples of the corresponding monomeric complex salts pressed onto indium foil.

UV−vis spectroscopy and spectroelectrochemical measurements were carried out by using a Hewlett-Packard Model 8451A diode array spectrophotometer interfaced to an IBM compatible PC. In measuring the absorption spectra of polymeric films, light scattering effects were minimized by including a clean ITO electrode in the reference scan. Spectroelectrochemical measurements were made with a 1 cm path length cuvette adapted with a Teflon top to position reproducibly the reference, counter (coiled Pt wire), and working ITO electrodes. Spectroelectrochemical data were analyzed by use of the program SPECFIT[25] which utilizes global factor analysis methods to interpret spectral changes and determine the number of colored components observed in an experiment.[26,27]

(23) Ingle, J. D., Jr.; Crouch, S. R. *Spectrochemical Analysis;* Prentice Hall, Inc.: Englewood Cliffs, NJ, 1988, pp 429−433.
(24) Shirley, D. A. *Phys. Rev. B* **1972**, *5*, 4709−4714.
(25) Binstead, R. A.; Zuberbühler, A. D. *Specfit Global Analysis* ver. 2.09U; Spectrum Software Associates, Chapel Hill, NC, 1995.

Results and Discussion

^{1}H NMR. Geometrical Isomers. ^{1}H NMR peak assignments for *cis*-$[Ru^{II}(vbpy)_2(py)_2](PF_6)_2$ (Experimental Section) are based on those for *cis*-$[Ru^{II}(bpy)_2(py)_2](BF_4)_2$.[28] Derivatization of the bipyridine rings results in three possible geometric isomers with regard to the relative positions of the vinyl substitutents and pyridine ligands (Scheme 3). The asterisk notation indicates protons on the aromatic rings of the bipyridine ligands which are adjacent to both pyridine ligands. These protons resonate at lower fields than those in corresponding positions on the opposite sides of the bipyridine ligands since they are not rigidly located above the plane of two aromatic rings. The pyridines are free to rotate around the Ru−N bond,[28] and the amount of shielding by the induced magnetic field of the π electrons of the aromatic rings is reduced. No attempt was made to separate the isomers by HPLC, and the monomer used for the electropolymerization can be assumed to be a mixture of the three.

Preparation of Polymeric Films. Thin films of poly$[Ru^{II}(vbpy)_2(py)_2](PF_6)_2$ were grown in acetonitrile solutions containing 1.0 mM of the monomer and 0.1 M TBAH by repeatedly cycling the potential of the working electrode between −0.5 and −1.7 V at either 50 mV/s for ITO or 100 mV/s for Pt disk electrodes. Reversible, ligand-based bipyridine reductions occur at $E^{o\prime} = -1.38$ and −1.57 V for the $[Ru(vbpy)_2(py)_2]^{2+/+}$ and $[Ru(vbpy)_2(py)_2]^{+/0}$ couples, respectively. Film surface coverages, Γ in mol/cm^2, were determined by measuring the charge (Q) passed under the cathodic wave of the $Ru^{III/II}$ couple ($E^{o\prime} = 1.23$ V) by using slow scan cyclic voltammetry in a fresh electrolyte-containing solution and eq 1, where $n = 1$, F is Faraday's constant, and A is the measured geometrical area of the electrode. Baseline corrections of cyclic voltammograms and numerical integration for determination of Q utilized a cubic-spline interpolation routine.[29]

$$\Gamma = Q/nFA \qquad (1)$$

Photochemical Ligand Loss. In Figure 1 are shown cyclic voltammograms in 0.1 M TBAH/CH_3CN at various times during broad band photolysis of poly$[Ru^{II}(vbpy)_2(py)_2]^{2+}$ ($\Gamma = 2 \times 10^{-8}$ mol/cm^2) on a Pt disk in a dichloromethane solution of 0.1 M TBACl. Before recording the cyclic voltamograms shown in Figure 1, the film was cycled once to 1.8 V to incorporate PF_6^- into the film as counterion and remove current response due to oxidation of residual chloride ion. Sequential formation of poly$[Ru^{II}(vbpy)_2(py)Cl]^+$ and poly$[Ru^{II}(vbpy)_2Cl_2]$ occurred as indicated by the loss of the wave for the bis-pyridine couple at $E^{o\prime} = 1.23$ V and the appearance of new waves at $E^{o\prime} = 0.73$ and 0.31 V. Conversion to the pyridine-chloro occurred predominantly within the first 60 s of photolysis (Figure 1a). Over the next 8 min, the wave for the poly$[Ru(vbpy)_2(py)Cl]^{2+/+}$ couple at +0.73 V was replaced by the wave for the poly-

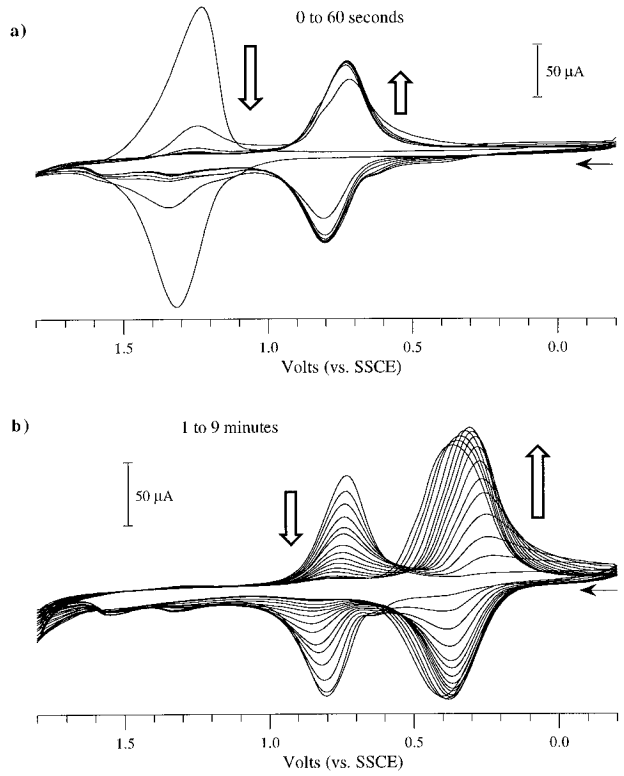

Figure 1. Cyclic voltammograms collected at various time intervals following photolysis of poly$[Ru(vbpy)_2(py)_2]^{2+}$ ($\Gamma = 2.0 \times 10^{-8}$ mol/cm^2) on a 0.12 cm^2 platinum disk electrode in a solution of 0.1 M TBACl/CH_2Cl_2. Cyclic voltammograms were recorded at 100 mV/s in 0.1 M TBAH/CH_3CN at various times during the photolysis.

$[Ru(vbpy)_2Cl_2]^{+/0}$ couple at 0.31 V (Figure 1b). Qualitatively, the first step is more efficient than the second, allowing for a rapid increase in the concentration of the pyridine-chloro in the film followed by slow conversion to the bis-chloro. Extended photolysis leads to complete substitution.

Plots of the relative surface coverages of each component as a function of photolysis time are shown in Figure 2. Surface coverages were calculated by integration of the reductive component of the $Ru^{III/II}$ waves. These plots show that there is a loss of net electroactivity by ~40% after conversion to the pyridine-chloro, followed by nearly complete recovery after formation of the bis-chloro. The loss of electroactivity can be attributed to "charge trapping" of redox sites during the intermediate stages in the photolysis.[30] Redox conduction occurs by electron-hopping and successive electron transfer reactions between neighboring sites.[3] The kinetics are governed by the potential applied to the working electrode and the concentration of oxidized and reduced sites in the film. In a partially photolyzed film, oxidation of poly$[Ru^{II}(vbpy)_2(py)Cl]^+$ to poly$[Ru^{III}(vbpy)_2(py)Cl]^{2+}$ is facilitated by self-exchange with neighboring pyridine-chloro sites but *not* by poly$[Ru^{III}(vbpy)_2Cl_2]^+$ since $E^{o\prime}(RuL_2Cl_2^{+/0}) < E^{o\prime}(RuL_2(py)Cl^{2+/+})$. Neighboring bis-pyridine sites would facillitate oxidation of isolated pyridine-chloro sites, but only at potentials approaching the poly$[Ru(vbpy)_2(py)_2]^{3+/2+}$ couple, resulting in an enhanced current or "prepeak" during the *first* oxidative cycle. This type of current response is often observed in cyclic voltamograms of bilayer film

(26) Binstead, R. A.; Stultz, L. K.; Meyer, T. J. *Inorg. Chem.* **1995**, *34*, 546−551.
(27) Malinowski, E. R. *Factor Analysis in Chemistry*, 2nd ed.; Wiley-Interscience: New York, 1991.
(28) Hitchcock, P. B.; Seddon, K. R.; Turp, J. E.; Yousif, Y. Z.; Zora, J. A.; Constable, E. C.; Wernberg, O. *J. Chem. Soc., Dalton Trans.* **1988**, 1837−1842.
(29) Press, W. H.; Flanny, B. P.; Teukolsky, S. A.; Vetterling, W. T. *Numerical Recipes, The Art of Scientific Computing;* Cambridge University Press: Cambridge, 1988.
(30) Denisevich, P.; Abruña, H. D.; Leidner, C. R.; Meyer, T. J.; Murray, R. W. *Inorg. Chem.* **1982**, *21*, 2153−2161.

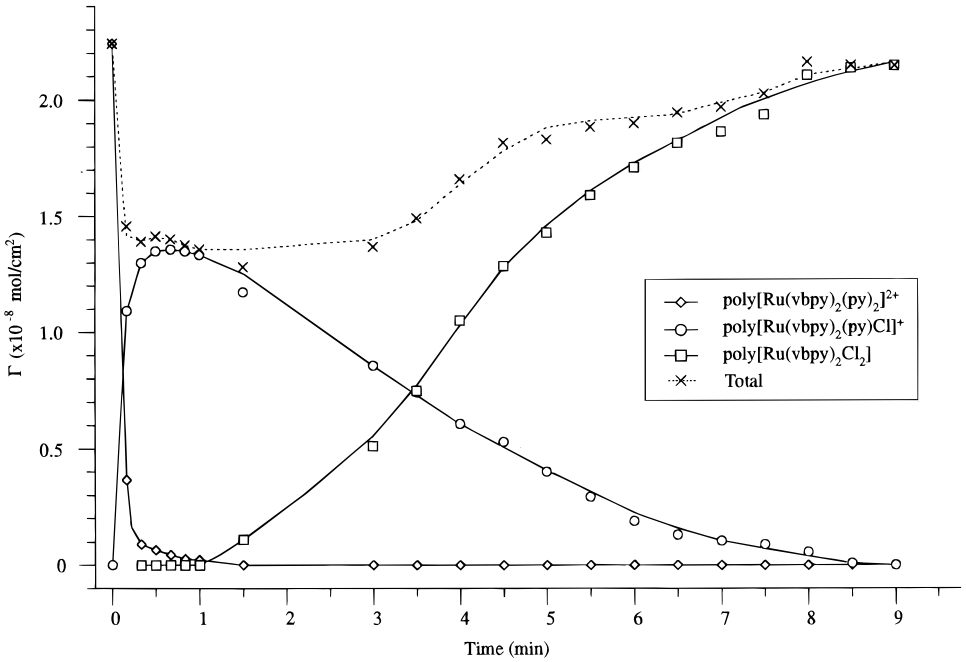

Figure 2. Surface coverages vs photolysis time for the three components of the film in Figure 1. The dashed line represents the total surface coverage by adding of the coverages for the three components at each sampling time.

assemblies.[31−34] In photosubstituted films, the oxidative prepeaks were obscured by current from oxidation of residual chloride in the films.

In either case, the mixed distribution of redox sites throughout the film results in an increased number of pyridine-chloro sites that become electrochemically isolated or "trapped" during the timescale of the voltammogram. At very slow sweep rates, the film should reach equilibrium and redox trapping should not be current limiting. Electroactivity of the film was restored once all of the sites were photochemically converted to the bis-chloro.

Reductive cycling of the pyridine-chloro and bis-chloro films to −2.0 V in acetonitrile led to rapid loss of the chloro ligands and formation of reversible $Ru^{III/II}$ couples for poly[$Ru(vbpy)_2(CH_3CN)Cl]^+$ at 0.79 V and poly[$Ru(vbpy)_2(CH_3CN)_2]^{2+}$ at 1.30 V. Reductively induced ligand substitution is well-established for related monomeric complexes in solution.[35]

Photosubstitution also occurs in "dry" films after incorporation of Cl^- as counterion by ion exchange. However, under these conditions, photolysis leads predominantly to poly[$Ru^{II}(vbpy)_2(py)Cl]^+$, even with irradiation times greater than 30 min. This can be attributed to the differences in quantum yields for photosubtitution[36] and the overall amount of chloride that can be incorporated in the polymeric matrix. Solvent swelling for wet films apparently allows for more efficient labilization of pyridine, and improved ion transport for incorporation of chloride.

FTIR Spectroscopy of Polymeric Films. In Figure 3a,b are shown specular reflectance infrared spectra of poly[$Ru^{II}(vbpy)_2(py)_2]^{2+}$ (as the PF_6^- and Cl^- salts, respectively) on a polished platinum flag before and

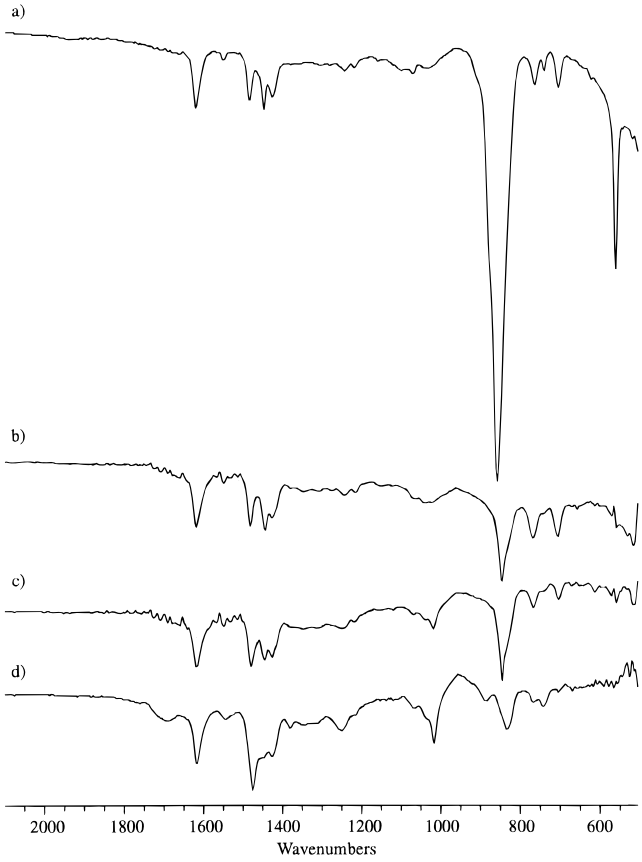

Figure 3. (a) Specular reflectance FTIR spectrum of poly[$Ru(vbpy)_2(py)_2](PF_6)_2$ ($\Gamma = 1.0 \times 10^{-8}$ mol/cm²) on a polished platinum flag electrode. In spectrum (b), Cl^- was incorporated as the counterion via ion exchange by soaking the film in an aqueous solution of 3 M NaCl for 2 h. Spectrum (c) was acquired after conversion of the the film to poly[$Ru(vbpy)_2(py)Cl]Cl$ by dry photolysis following Cl^- incorporation. Spectrum (d) was acquired after conversion of the the film to poly[$Ru(vbpy)_2(Cl)_2$] by a second photolysis in 0.1 M $TBACl/CH_2Cl_2$. The compositions of the films in spectra (c) and (d) were verified by cyclic voltammetry.

(31) Abruña, H. D.; Denisevich, P.; Umaña, M.; Meyer, T. J. *J. Am. Chem. Soc.* **1981**, *103*, 1−5.
(32) Denisevich, P.; Williams, K. W.; Murray, R. W. *J. Am. Chem. Soc.* **1981**, *103*, 4727−4737.
(33) Pickup, P. G.; Leidner, C. R.; Denisevich, P.; Murray, R. W. *J. Electroanal. Chem.* **1984**, *164*, 39−61.
(34) Leidner, C. R.; Murray, R. W. *J. Am. Chem. Soc.* **1985**, *107*, 551−556.
(35) Sullivan, B. P.; Conrad, D.; Meyer, T. J. *Inorg. Chem.* **1985**, *24*, 3640−3645.
(36) Pinnick, D. V.; Durham, B. *Inorg. Chem.* **1984**, *23*, 1440−1445.

Table 1. Formal Potentials (±0.02 V) vs SSCE in 0.1 M TBAH/CH_3CN at 25 °C

film	$E°'$ ($M^{III/II}$)	$E°$ ($bpy^{0/-}$)$_1$	$E°'$ ($bpy^{0/-}$)$_2$
poly[Ru(vbpy)$_2$(py)$_2$]$^{2+}$	1.27	−1.64	−1.83
poly[Ru(vbpy)$_2$(py)Cl]$^{+}$	0.77		
poly[Ru(vbpy)$_2$Cl$_2$]	0.35		
poly[Ru(vbpy)$_2$(CH_3CN)$_2$]$^{2+}$	1.34	−1.47	−1.60
poly[Ru(vbpy)$_2$(CH_3CN)Cl]$^{2+}$	0.83		

Table 2. FTIR Bands and Assignments in Dry Films on a Platinum Flag Electrode

[Ru(py)$_2$]-(PF_6)$_2$[a]	[Ru(py)$_2$]Cl$_2$	[Ru(py)Cl]Cl[b]	[$RuCl_2$][c]	assignment[d]
1619	1618	1618	1616	ν(C=N, bpy)
1483	1481	1479	1475	ν(bpy)
1448	1444	1444	1451	ν(bpy)
1425	1425	1425	1427	ν(bpy)
		1245	1249	δ(CH) + ν(bpy)
		1016	1016	ring breathing
856				PF_6^-
	844	844	831	γ(CH)
761	765	765	765	ν(bpy)
738	738	738	740	ν(bpy)
703	703	702		ν(pyridine)
559				PF_6^-

[a] [Ru(py)$_2$]$^{2+}$ is poly[Ru(vbpy)$_2$(py)$_2$]$^{2+}$. [b] [Ru(py)Cl]$^{+}$ is poly-[Ru(vbpy)$_2$(py)Cl]$^{+}$. [c] [$RuCl_2$] is poly[Ru(vbpy)$_2$Cl$_2$]. [d] ν = stretch, δ = in-plane deformation, γ = out-of-plane deformation.

after soaking for 2 h in a dichloromethane solution of 0.1 M TBACl. Complete ion exchange occurred as indicated by the disappearance of the PF_6^- stretches at 559 and 856 cm^{-1}. Similar results were obtained by soaking the films in aqueous solutions of NaCl. Spectra of the pyridine-chloro and bis-chloro films are also shown in Figure 3. Cyclic voltammetry was used to confirm the composition of the photosubstituted films after aquiring the FTIR spectra.

In comparing the spectra, there is relatively little change in the pattern of ν(bpy) ring stretching bands between 1425 and 1618 cm^{-1} or the lower energy ν(bpy) bands at 765 and 738 cm^{-1}. The ν(pyridine) band at 703 cm^{-1} decreases in intensity in the pyridine-chloro film and disappears in the bis-chloro spectra. The FTIR band assignments in Table 2 were made by comparing the spectra to those of salts of related monomeric Ru−bpy and Ru−py complexes.[37−39]

Photolithography and Image Formation. Spatially resolved photosubstitution was achieved by contact lithography[40] and photolysis of dry films in the absence of external solvent, as illustrated in Figure 4a. Prior to photolysis, the films were soaked for 2 h or longer in aqueous solutions containing 3 M NaCl. Typical photolysis times were 5−10 min. Figure 4b illustrates the spatial electrochromism of the assembly effected by controlling the potential of the underlying electrode and is discussed in more detail in subsequent sections.

In Figure 5 are shown optical microscope photographs of an imaged film on a 4 mm diameter platinum disk electrode. The lighter areas are poly[Ru^{II}(vbpy)$_2$(py)$_2$]$^{2+}$ and the darker, photolyzed regions, poly[Ru^{II}(vbpy)$_2$(py)-Cl]$^{+}$. The lines at group 4-1 in Figure 4b have widths of ca. 30 μm and are clearly discernible. Higher resolution

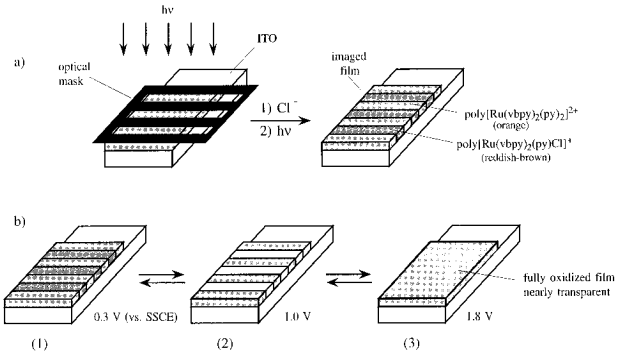

Figure 4. (a) Schematic representation of the photolithographic process used to image poly[Ru(vbpy)$_2$(py)$_2$]Cl$_2$ on an ITO electrode. The dark features of the imaged film represent poly[Ru(vbpy)$_2$(py)Cl]$^{+}$ formed in the irradiated regions of the initial film. (b) Potential control of the underlying ITO electrode allows for selective oxidation and spatially controlled color changes in the bicomponent film.

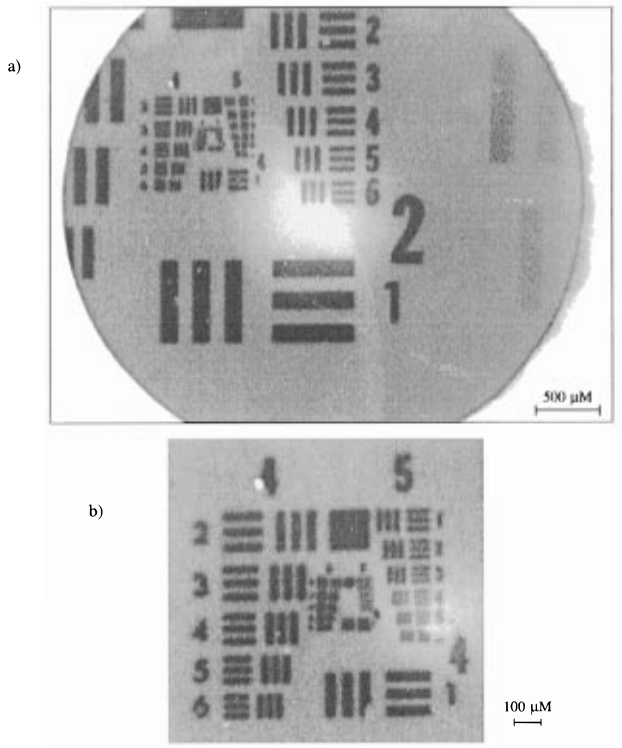

Figure 5. Optical micrographs of an imaged film ($\Gamma = 5.0 \times 10^{-8}$ mol/cm^2) composed of poly[Ru(vbpy)$_2$(py)$_2$](PF$_6$)$_2$ (lighter regions) and poly[Ru(vbpy)$_2$(py)Cl](PF$_6$) (darker regions) on a 4.0 mm diameter platinum disk electrode. The edges of the electrode are apparent in (a). The size of the imaged pattern corresponds well to the optical mask used to generate the image. The lines at group 2-1 have widths of 125 μm. The higher magnification image in (b) shows line groups of elements 4 and 5. The lines at group 5-1 have widths of ca. 15 μm.

line patterns having widths smaller than 10 μm could also be distinguished.

XPS Analysis of a Bicomponent Film. Small-spot XPS was used to analyze a spatially resolved, bicomponent film ($\Gamma = 1.2 \times 10^{-8}$ mol/cm^2) of ~70% poly[Ru^{II}-(vbpy)$_2$(py)$_2$](PF$_6$)$_2$ and ~30% poly[Ru^{II}(vbpy)$_2$(py)Cl]-(PF$_6$), as determined by cyclic voltammetry. During the photolysis step, an optical mask was positioned such that approximately half of the 4.0 mm diameter Pt disk electrode was irradiated. Cyclic voltammetry in fresh electrolyte solution was used to determine the overall

(37) Krause, R. A. *Inorg. Chim. Acta* **1977**, *22*, 209−213.
(38) Krause, R. A. *Inorg. Chim. Acta* **1978**, *31*, 241−242.
(39) Poizat, O.; Sourisseau, C. *J. Phys. Chem.* **1984**, *88*, 3007−3014.
(40) Wolf, S.; Tauber, R. N. *Silicon Processing for The VLSI Era;* Lattice Press: Sunset Beach, CA, 1986; Vol. 1, pp 468−469.

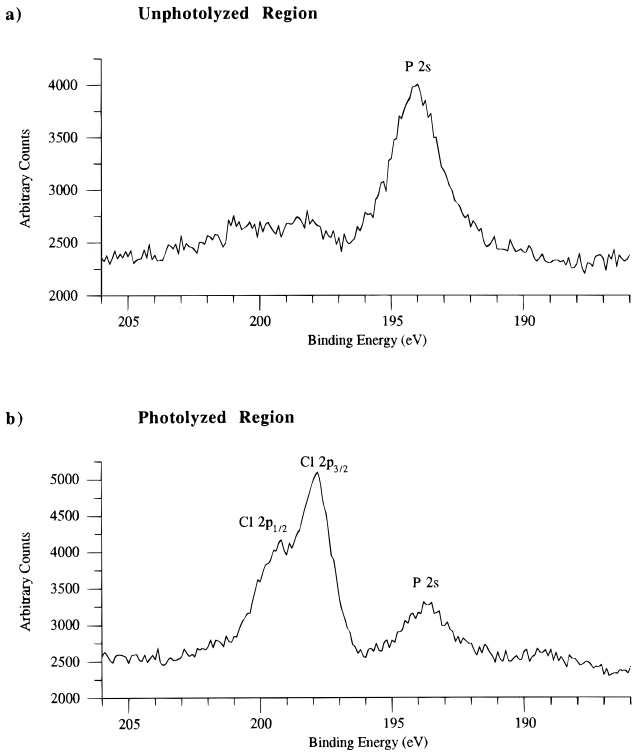

Figure 6. XPS for the Cl 2p and P 2s peaks of a photoimaged, polymer-coated electrode ($\Gamma = 2.1 \times 10^{-8}$ mol/cm^2) consisting of ca. 70% poly[Ru(vbpy)$_2$(py)$_2$]$^{2+}$ and 30% poly[Ru(vbpy)$_2$(py)Cl]$^+$ in the (a) unphotolyzed and (b) photolyzed regions, respectively.

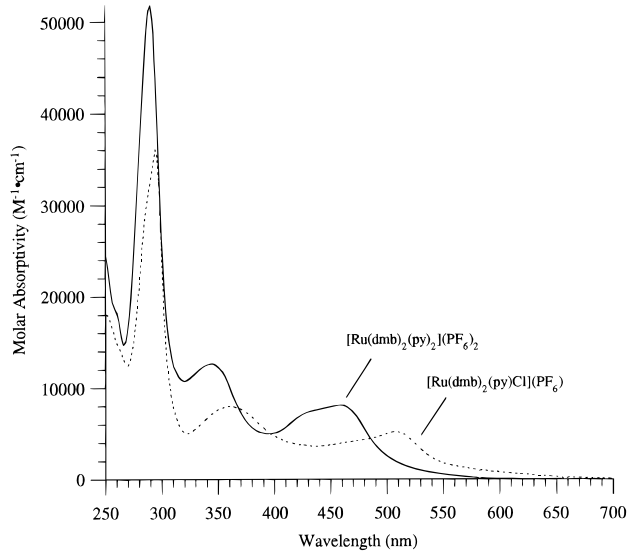

Figure 7. Electronic absorption spectra of [Ru(dmb)$_2$(py)$_2$]-(PF$_6$)$_2$ and [Ru(dmb)$_2$(py)Cl](PF$_6$)·H$_2$O in CH$_2$Cl$_2$.

composition of the film and to reincorporate PF_6^- as the counterion. During the XPS analysis, tin foil was used to cover areas not analyzed to prevent possible X-ray photodegradation and detection of photoelectrons from unwanted regions.

XPS spectra from 186 to 206 eV are shown in Figure 6 for the unphotolyzed and photolyzed regions of the film. Peaks for P 2s and the Cl 2p doublet appear in this region. Photoelectron peaks for F 1s (686.1 eV), N 1s (400.0 eV), and Ru 3d$_{5/2}$ (281.0 eV) were observed in survey scans. Binding energies and calculated atomic percentages are reported in Table 3. Ratios of the experimental and predicted atomic percentages are reported in Table 4.

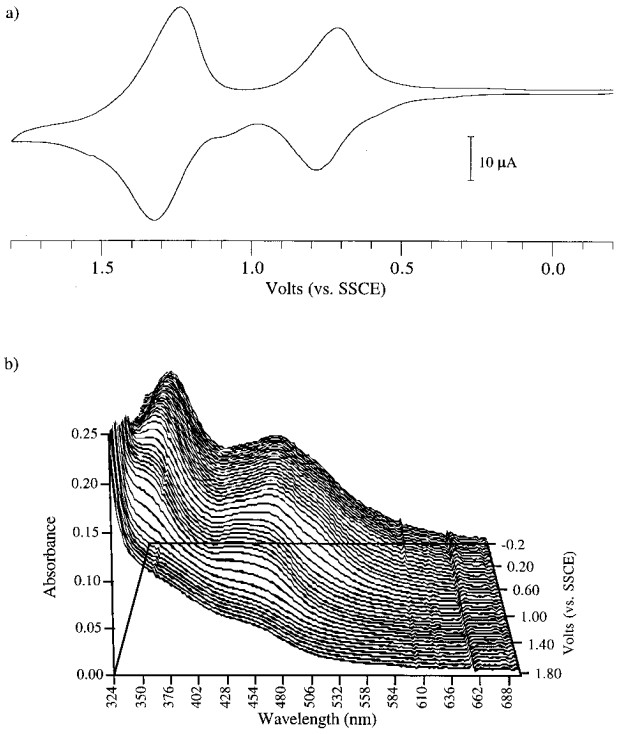

Figure 8. (a) Cyclic voltammogram of a bicomponent film imaged as in Figure 4 on an optically transparent ITO electrode in 0.2 M TBAH/CH$_2$Cl$_2$. The scan rate was 5 mV/s. The overall composition of the film was calculated to be ca. 60% poly[Ru(vbpy)$_2$(py)$_2$]$^{2+}$ and 40% poly[Ru(vbpy)$_2$(py)Cl]$^+$ with an overall surface coverage of 1.2×10^{-8} mol/cm^2. (b) Spectroelectrochemical data aquired during the oxidative sweep of the cyclic voltammogram in (a).

Table 3. Photoelectron Binding Enegies (±0.2 eV) and Calculated Atomic Percentages

	poly[Ru(vbpy)$_2$(py)$_2$](PF$_6$)$_2$			
	unphotolyzed		photolyzed	
photoelectron peak	BE (eV)	atomic %	BE (eV)	atomic %
F 1s	686.1	17.6	686.2	9.4
N 1s	400.0	9.6	399.9	9.6
Ru 3d$_{5/2}$	281.0	1.5	280.8	1.5
Cl 2p$_{1/2}$	199.0		199.0	
Cl 2p$_{3/2}$	197.4	0.2[a]	197.4	1.5[a]
P 2s	193.3	2.9	193.3	1.2

[a] The atomic percentage for Cl was calculated by using the combined integrated areas for the Cl 2p$_{1/2}$ and Cl 2p$_{3/2}$ peaks, and the appropriate RSF normalization factor.

Table 4. Ratios of Calculated Atomic Percentages for Bicomponent Film XPS Analysis

	poly[Ru(vbpy)$_2$(py)$_2$](PF$_6$)$_2$			
	unphotolyzed		photolyzed	
ratio	measured	predicted	measured	predicted
P/Ru	2.0	2	0.8	1
F/Ru	11.7	12	6.3	6
F/P	6.0	6	7.9	6
F/Cl	72.4	∞	6.2	6
Cl/ Ru	0.2	0	1.0	1
N/Ru	6.5	6	6.4	5

The atomic percentages support monosubstitution and formation of poly[Ru(vbpy)$_2$(py)Cl](PF$_6$) in the photolyzed region of the film. The ratio of PF_6^- to Ru decreases by ~1/2 and the ratio of Cl/Ru increases. The detection of residual chloride in the unphotolyzed area may be a consequence of the high surface sensitivity of XPS and the exposure of the sample to ambient light either before or after the photolysis while Cl^- was still

incorporated as the counterion. The nitrogen content does not undergo a significant change after photolysis, suggesting retention of pyridine at least within surface layers of the polymeric network. The slightly elevated nitrogen signals, compared to predicted values, cannot be attributed to adsorbed or incorporated electrolyte, since the N 1s binding energies of quaternatry ammonium salts are approximately 2 eV higher in energy than those of the heterocyclic nitrogen atoms of the pyridyl ligands.

Spatial Electrochromism. A bicomponent film ($\Gamma = 2.1 \times 10^{-8}$ mol/cm^2) was prepared on an optically transparent ITO electrode by dry photolysis and imaging. The composition of the film was determined by cyclic voltammetry, Figure 8a, to be 60% poly[$Ru(vbpy)_2(py)_2$]$^{2+}$ and 40% poly[$Ru(vbpy)_2(py)Cl$]$^+$. The optical mask was a gradient Ronchi ruling with line widths ranging from 100 to 500 μm. A schematic diagram showing the formation of the film pattern and its subsequent response to redox potential cycling is shown in Figure 4.

UV−visible spectra of the model complexes [$Ru^{II}(dmb)_2(py)_2$]$(PF_6)_2$ and [$Ru^{II}(dmb)_2(py)Cl$]$(PF_6)\cdot H_2O$ are shown in Figure 7 for comparison with those of the bicomponent film. Absorption changes in the bicomponent film were monitored by transmittance measurements at various applied potentials during the oxidative sweep (5 mV/s) of the cyclic voltammogram in Figure 8a. At 0.30 V, MLCT absorptions for both bis-pyridine and pyridine-chloro complexes were present with maxima at 350 and 464 nm (Figure 8b). The shoulder at ca. 510 nm is due to the lower energy MLCT band for the pyridine-chloro complex. By 1.0 V, selective oxidation of poly[$Ru^{II}(vbpy)_2(py)Cl$]$^+$ to poly[$Ru^{III}(vbpy)_2(py)Cl$]$^{2+}$ had occurred with loss of its Ru^{II} MLCT absorption bands. In Figure 8b, the low-energy shoulder disappears and the peak maxima shift to higher energy. The spectrum closely resembles that of poly[$Ru^{II}(vbpy)_2(py)_2$]$^{2+}$ with maxima at ~340 and 434 nm. Subtraction of the spectrum at 1.0 V from the 0.3 V spectrum gave maxima at 312 and 506 nm corresponding to poly[$Ru^{II}(vbpy)_2(py)Cl$]$^+$. At 1.8 V, oxidation of the bis-pyridine complex resulted in loss of the remaining MLCT absorptions and bleaching of the film. On a subsequent reductive sweep the absorption changes were reversed with the initial absorption spectrum being recovered.

In Figure 9 are shown plots of the absorbance (at 450 nm) vs applied potential for a similarly prepared bicomponent film ($\Gamma = 1.2 \times 10^{-8}$ mol/cm^2, ca. 45% poly[$Ru(vbpy)_2(py)_2$]$^{2+}$ and 55% poly[$Ru(vbpy)_2(py)Cl$]$^+$) recorded during the first, fifth, and tenth potential cycles at 2 mV/s. Individual absorbance measurements were recorded every 50 mV and are represented by the open circles for the forward scan with open triangles for the reverse scan. Absorbance values correlate well for both the oxidative and reductive sweeps. In the later cycles, a slight hysteresis developed and absorbance values for the return, reductive, sweep were lower than those observed at corresponding potentials during the oxidative sweep. The hysteresis was greatest at potentials near the two redox couples and is less pronounced near the limits of the potential sweeps. This may be indicative of reduced charge transport within the film with

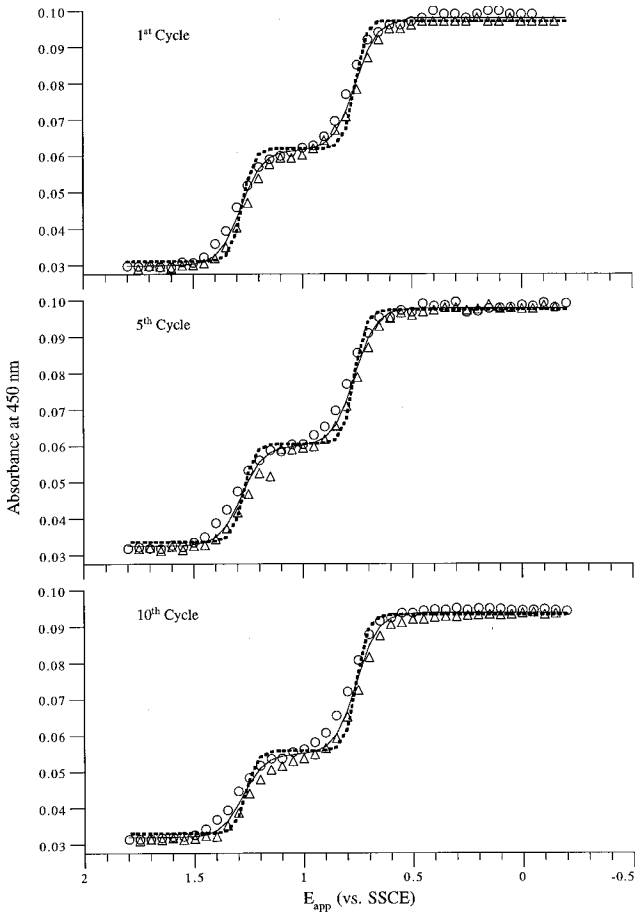

Figure 9. Absorbance (at 450 nm) vs applied potential for an imaged, bicomponent film on an ITO electrode ($\Gamma = 1.2 \times 10^{-8}$ mol/cm^2, ca. 45% poly[$Ru(vbpy)_2(py)_2$]$^{2+}$ and 55% poly[$Ru(vbpy)_2(py)Cl$]$^+$) recorded during the first, fifth, and tenth potential cycles at 2 mV/s. Individual absorbance measurements are indicated by the open circles for the forward scan and open triangles (Δ) for the reverse scan. The dashed line is the theoretical Nernstian response. The solid line represents the modified Nernstian fit calculated by using an interaction parameter of $g = 0.51$ (eq 2).

continuous cycling. However, variations in experimental conditions are known to influence the electrochemical response of redox films through such variables as electrode prehistory, the time scale of the experiment, and the choice of suitable counterions and solvent.[41]

The theoretical Nernstian response for the bicomponent film is represented by the dashed line and formal potentials for the two couples taken as 1.27 V and 0.76 V. Even at the relatively slow potential sweep rate of 2 mV/s, the redox behavior of the film is non-Nernstian as indicated by the broad wave shapes for the two couples. Similar behavior has been observed in polyanionic films of Nafion containing $Ru(bpy)_3^{2+}$ and attributed to interactions between redox sites in densely populated polymeric matrixes.[42] Broadening in cyclic voltammograms of derivatized electrodes has been suggested to arise from differences in the surface activities of the redox species.[43,44] Equivalently, the films can be thought of as containing a Gaussian distribution of

(41) Hillman, A. R.; Bruckenstein, S. *J. Chem. Soc., Faraday Trans.* **1993**, *89*, 339−348.
(42) Buttry, D. A.; Anson, F. C. *J. Am. Chem. Soc.* **1982**, *104*, 4824−4829.
(43) Brown, A. P.; Anson, F. C. *Anal. Chem.* **1977**, *49*, 1589−1595.
(44) Ikeda, T.; Leidner, C. R.; Murray, R. W. *J. Electroanal. Chem.* **1982**, *138*, 343−365.

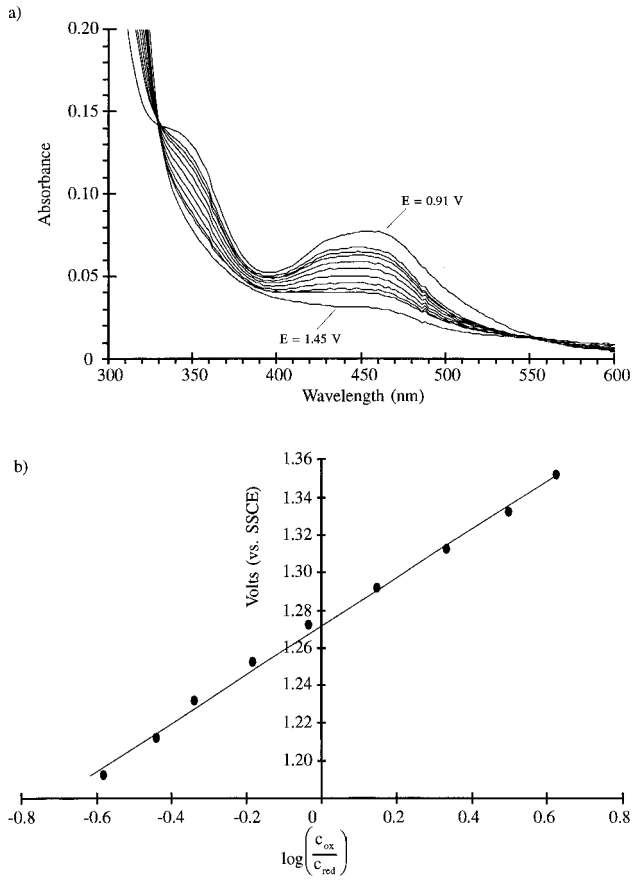

Figure 10. (a) Spectroelectrochemistry of a homogeneous film of poly[Ru(vbpy)$_2$(py)$_2$]$^{3+/2+}$ ($\Gamma = 7.8 \times 10^{-9}$ mol/cm^2) on an ITO electrode. Absorption spectra were aquired between 0.90 and 1.45 V in 20 mV increments. (b) Nernst plot for the Ru$^{III/II}$ couple prepared from absorbance−potential data 450 nm (●).

surface states with different formal potentials.[45] A simplified correction to the Nernst equation can be made by incorporation of an empirical interaction parameter, g, as shown in eq 2.[46]

$$E = E^{o\prime} + \frac{RT}{gnF}\ln\left(\frac{[\text{ox}]}{[\text{red}]}\right) \qquad (2)$$

To investigate this point in more detail and ensure that the broadening was not an artifact of slow interfacial electrode kinectics, the spectroelectrochemistry of a homogeneous film of poly[Ru(vbpy)$_2$(py)$_2$]$^{3+/2+}$ ($\Gamma = 7.8 \times 10^{-9}$ mol/cm^2) was monitored while applying controlled potential steps in 20 mV increments to the working electrtode. At each potential the absorption spectrum was monitored until it became constant (5−10 min), at which point the current passing had fallen to background levels. Absorbance−potential data at 450 nm were used to prepare the Nernst plot shown in Figure 10b. The plot is linear with an intercept of 1.27 V, which corresponds to the expected formal potential of the poly[Ru(vbpy)$_2$(py)$_2$]$^{3+/2+}$ couple. Linear regression yields a slope of 128 mV/decade which is significantly larger than the 59 mV/decade expected for an ideal redox couple ($g = 1$) and correlates to an interaction parameter of $g = 0.46$. Incorporation of this term into the modified Nernst expression, eq 2, yields significantly better fits for the absorbance vs applied potential plots in Figure 9 as represented by the solid lines.

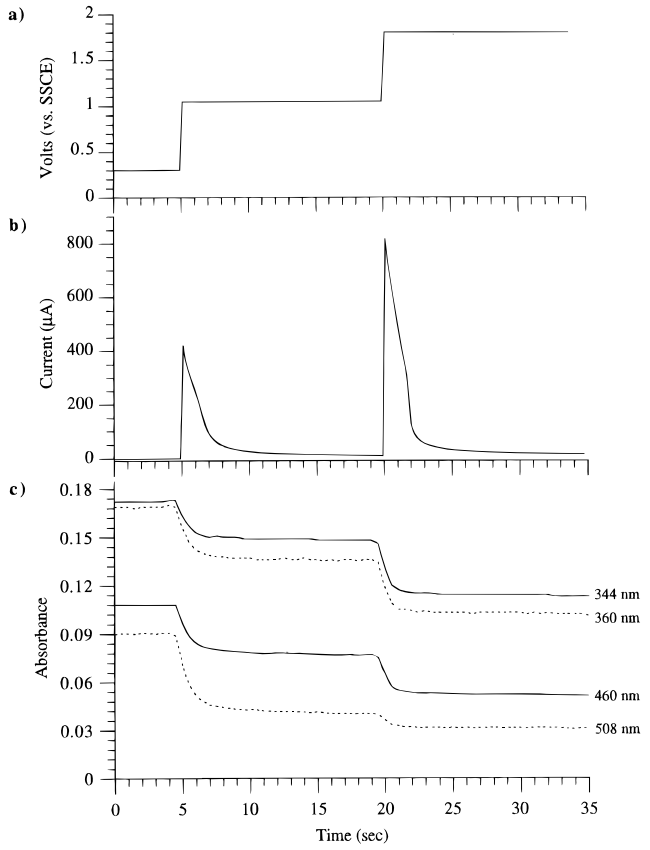

Figure 11. Chronoamperometry of the film in Figure 8. (a) Potential vs time plot. (b) Current vs time plot. (c) Absorption vs time plots at 344, 460 nm (—) and 360, 508 nm (- - -).

In Figure 11 is shown the chronoamperometric response for the same bicomponent film as in Figure 8. The potential of the ITO electrode was stepped from 0.3 to 1.0 V and then from 1.0 to 1.8 V as shown in Figure 11a. The current responses in Figure 11b correspond to successive oxidations of the pyridine-chloro and bispyridine components. The distorted current transients are due to high ohmic resistance caused by either the low electrolyte concentration or the intrinsically large resistance of the ITO electrode.[47] Absorbance changes (Figure 11c) were monitored at the MLCT maxima for each component; 360 and 508 nm for poly[Ru(vbpy)$_2$(py)Cl]$^+$ and 344 and 460 nm for poly[Ru(vbpy)$_2$(py)$_2$]$^{2+}$. The current decays and corresponding drops in the absorption spectra demonstrate relatively rapid switching of redox states for both components in the film.

Conclusions

This work demonstrates the use of photosubtitution in thin, electropolymerized films of poly[Ru(vbpy)$_2$(py)$_2$]$^{2+}$ to fabricate spatially resolved, bicomponent film assemblies. Lithographic techniques can be used to pattern films with separate regions containing either poly[Ru(vbpy)$_2$(py)$_2$]$^{2+}$ or poly[Ru(vbpy)$_2$(py)Cl]$^+$. Ligand exchange of Cl$^-$ for pyridine causes a shift in formal potential of the Ru$^{III/II}$ couple from 1.27 to 0.77 V vs SSCE. By controlling the potential of the underlying

(45) Albery, W. J.; Boutelle, M. G.; Colby, P. J.; Hillman, A. R. *J. Electroanal. Chem.* **1982**, *133*, 135−145.
(46) Pickup, P. G.; Kutner, W.; Leidner, C. R.; Murray, R. W. *J. Am. Chem. Soc.* **1984**, *106*, 1991−1998.
(47) Daum, P.; Murray, R. W. *J. Phys. Chem.* **1981**, *127*, 389−396.

electrode, selective oxidation of one or both components occurs, allowing for spatially resolved color changes in imaged films. By using this approach, it is possible to fabricate patterned, multicomponent, electrochromic devices with relatively minimal processing of the film or the underlying substrate.

Acknowledgment. We gratefully acknowledge the U. S. Army Research Office under grants No. DAAL03-90-G-0062 and DAAL03-92-G-D166 for support of this work, Thomas R. Boussie for developing synthetic procedures for the preparation of 4-vinyl-4′-methyl-2,2′-bipyridine, George M. Coia for encoding much of the software used in the collection and analysis of the electrochemical data, and Robert A. Binstead for aid in the analysis and interpretation of spectroelectrochemical data.

CM950371S